[3]M. Fred, F. S. Tomkins, J. K. Brody, and M. Hamermesh, Phys. Rev. 82, 406 (1951).
[4]M. Gross, C. Fabre, P. Pillet, and S. Haroche, Phys. Rev. Lett. 36, 1035 (1976).
[5]J. C. MacGillivray and M. S. Feld, Phys. Rev. A 14, 1169 (1976).
[6]F. Gounand, M. Hugon, P. R. Fournier, and J. Berlande, J. Phys. B 12, 547 (1979).
[7]D. Rapp and W. E. Francis, J. Chem. Phys. 37, 2631 (1962); D. P. Hodgkinson and J. S. Briggs, J. Phys. B 9, 255 (1976).
[8]R. D. Rundel, D. E. Nitz, K. A. Smith, M. W. Geis, and R. F. Stebbings, Phys. Rev. A 19, 33 (1979).
[9]C. A. Kocher and A. J. Smith, Phys. Rev. Lett. 39, 1516 (1977).
[10]T. F. Gallagher and W. E. Cooke, Phys. Rev. A 19, 2161 (1979).
[11]R. S. Berry and S. E. Nielsen, Phys. Rev. A 1, 383, 395 (1970); S. E. Nielsen and R. S. Berry, Phys. Rev. A 4, 865 (1971).

# Emission Spectra of Core Excited Even-Parity $^2P$ States of Neutral Lithium

J. R. Willison, R. W. Falcone, J. C. Wang, J. F. Young, and S. E. Harris
*Edward L. Ginzton Laboratory, Stanford University, Stanford, California 94305*
(Received 13 February 1980)

Doubly excited even-parity $1snpmp\ ^2P$ states of neutral Li are metastable against autoionization and have large radiative yields. An emission spectrum from 160 Å to 250 Å of a high-power-microwave–heated Li plasma is reported. The spectrum, which differs substantially from that obtained in absorption, exhibits several new series as well as the phenomena of radiative autoionization.

PACS numbers: 32.30.Rj, 32.80.Dz, 52.50.Jm, 52.70.Kz

Optical transitions which originate from doubly excited even-parity $^2P$ states of neutral Li are good candidates for lasers in the 200-Å region of the spectrum.[1] Although the upper levels of these transitions lie about 60 eV above the first ionization potential, a combination of parity and angular-momentum selection rules prohibit their decay by Coulombic autoionization, and allow radiative yields. The strongest of these transitions, $1s2p^2\,^2P \rightarrow 1s^22p\,^2P^\circ$ (Fig. 1), occurs at 207.45 Å and was first observed by Buchet, Buchet-Poulizac, and Berry[3] by beam-foil excitation. It has a calculated[2,4,5] oscillator strength, Einstein $A$ coefficient, and branching ratio of $f_{12} = 0.13$, $A_{21} = 1.97 \times 10^{10}\ \text{sec}^{-1}$, and 0.83, respectively.

In this Letter we describe the emission spectrum of a microwave-heated Li plasma. The spectrum is dominated by radiative transitions from even-parity nonautoionizing $1snpmp\ ^2P$ upper levels to $1s^2qp\ ^2P^\circ$ lower levels and thus differs appreciably from spectra obtained either by optical absorption,[6-8] or by ejected-electron spectroscopy.[9,10]

The emission source consisted of a 20-cm-long section of stainless steel $X$-band waveguide containing Li and heated to 650 °C, corresponding to a Li density of about $10^{15}$ atoms/cm$^3$. A buffer gas of He at a pressure of 10 $\mu$m was used to help confine the Li vapor to the hot zone, and the waveguide was lined with a fine stainless steel screen to promote recirculation of the molten Li. The active region was viewed through a 7-mm-i.d., 20-cm-long tube which was soldered onto a hole in an elbow in the waveguide. The rf power was carried through this elbow into the Li waveguide heat pipe from a pulsed magnetron operating at 9.4 GHz with a peak power of about 200 kW, a 2-$\mu$s pulse width, and a 448-Hz repetition rate. Avalanche breakdown of the Li vapor occurred about

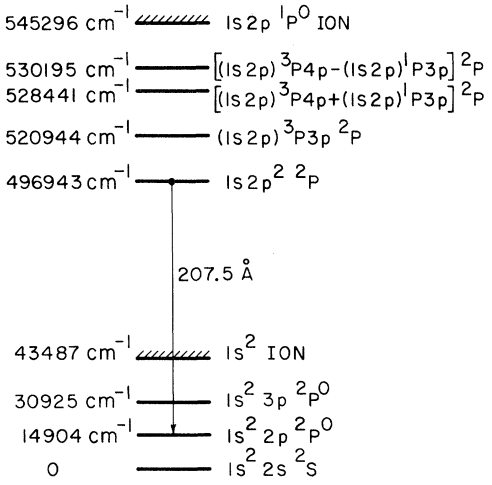


FIG. 1. Energy level diagram of neutral Li (Ref. 2).

 

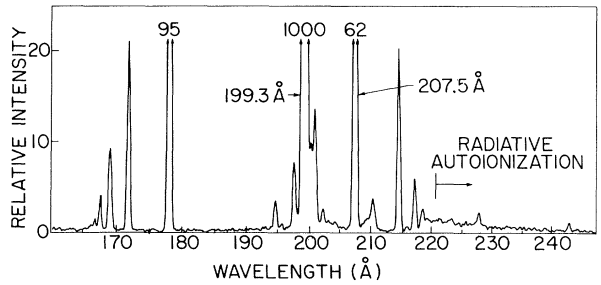


FIG. 2. Emission spectrum of Li.

400 ns after the start of the rf pulse, and vacuum ultraviolet (vuv) emission lasted for the remainder of the rf pulse.

Spectra were taken with a McPherson Model 247 grazing-incidence spectrometer operating in first order with a 300-line/mm grating at an 84° angle of incidence having a resolution of about 0.4 Å. vuv photons were detected by an EMI Model D233B electron multiplier followed by fast amplifiers, a pulse-height discriminator, and a counter which was gated on during the rf pulse. A minicomputer was programmed to read and reset the counter at 1-s intervals as the spectrometer was continuously scanned. Typically, we scanned the spectrometer at 0.05 Å/s and so 33 min were required to scan from 150 to 250 Å. After a scan the data were recorded on a magnetic disk, smoothed to reduce statistical noise, and plotted. The count rate for 207 Å was about $10^3$ per second, or about two counts per rf pulse. We estimate our detection efficiency to be about $10^{-10}$ based on a geometrical loss of $10^{-8}$ and assumed grating and phototube efficiency of 0.1 each. At an rf duty factor of $10^{-3}$, this implies a source rate of $10^{16}$ photons per second at 207 Å while the microwave power is on.

A spectral scan from 160 to 250 Å is shown in Fig. 2. The strongest line in the spectrum is the resonance line of Li II at 199.3 Å, which we used for wavelength calibration. Table I shows the observed wavelengths corresponding to even-parity core excited transitions, grouped in series characterized by a common upper level. The assignments and calculated wavelengths are based on a recent paper by Bunge.[2] We call particular attention to the series $1s2p^2\,{}^2P \rightarrow 1s^2np\,{}^2P^\circ$ which is reported here for the first time. The relative amplitudes of the series members differ somewhat from the recent calculation of Nicolaides and Beck[5] because of the radiative trapping by the large lower-state populations which are present in the plasma. For $n$ greater than 5, the series is not resolved and merges with radiative transitions to the $1s^2\,{}^1S + e^-$ continuum states. In these transitions, termed radiative autoionization or radiative Auger transitions, a small fraction of

TABLE I. Transitions from core excited $^2P$ states in neutral lithium.

| Observed wavelength (± 0.1 Å) | Relative intensity | Transition | Calculated[a] wavelength |
|---|---|---|---|
| 207.5[b-d] | 62 | $1s2p\,{}^2\,{}^2P \rightarrow 1s^2 2p\ {}^2P^\circ$ | 207.45 |
| 214.6 | 12 | $\rightarrow 1s^2 3p\ {}^2P^\circ$ | 214.58 |
| 217.1 | 6 | $\rightarrow 1s^2 4p\ {}^2P^\circ$ | 217.16 |
| 218.4 | 2 | $\rightarrow 1s^2 5p\ {}^2P^\circ$ | 218.37 |
| 220.5[e] | | $\rightarrow 1s^2\,{}^1S + e^-$ | |
| 197.8[c,d] | 8 | $(1s2p)\,{}^3P 3p\ {}^2P \rightarrow 1s^2 2p\ {}^2P^\circ$ | 197.61 |
| 194.8[c,d] | 3 | $[(1s2p)\,{}^3P 4p + (1s2p)\,{}^1P 3p]\,{}^2P \rightarrow 1s^2 2p\ {}^2P^\circ$ | 194.72 |
| 201.0 | 10 | $\rightarrow 1s^2 3p\ {}^2P^\circ$ | 200.99 |
| 203.3 | 0.3 | $\rightarrow 1s^2 4p\ {}^2P^\circ$ | 203.26 |
| 204.3 | 0.2 | $\rightarrow 1s^2 5p\ {}^2P^\circ$ | 204.32 |
| 200.3 | 8 | $[(1s2p)\,{}^3P 4p - (1s2p)\,{}^1P 3p]\,{}^2P \rightarrow 1s^2 3p\ {}^2P^\circ$ | 200.29 |
| 202.5 | 1.5 | $\rightarrow 1s^2 4p\ {}^2P^\circ$ | 202.54 |

[a] Calculation by Bunge (Ref. 2).
[b] Previously observed in emission (Ref. 3).
[c] Previously observed by two-photon absorption (Ref. 7).
[d] Previously observed by two-photon absorption (Ref. 8).
[e] Radiative autoionization tail extends to 240 Å.

TABLE II. Additional spectral features.

| Observed wavelength (Å ± 0.1) | Relative intensity | Transition |
|---|---|---|
| 166.4[a] | 1 | Li II $1s7p\ ^1P^\circ \rightarrow 1s^2\ ^1S$ |
| 167.2[a] | 4 | Li II $1s6p\ ^1P^\circ \rightarrow 1s^2\ ^1S$ |
| 168.7[a] | 10 | Li II $1s5p\ ^1P^\circ \rightarrow 1s^2\ ^1S$ |
| 171.7[a,b] | 21 | Li II $1s4p\ ^1P^\circ \rightarrow 1s^2\ ^1S$ |
| 177.9[a,b] | 95 | Li II $1s3p\ ^1P^\circ \rightarrow 1s^2\ ^1S$ |
| 199.3[a,b] | 1000 | Li II $1s2p\ ^1P^\circ \rightarrow 1s^2\ ^1S$ |
| 195.8[a] | 1 | Li I $(1s2s\ ^3S)4p\ ^2P^\circ \rightarrow 1s^2 2s\ ^2S$ |
| 209.6[a,d] | 2 | Li I $1s2s3d \rightarrow 1s^2 2p\ ^2P^\circ$ |
| 210.3[a,c] | 4 | Li I $1s(2s2p\ ^3P)\ ^2P^\circ \rightarrow 1s^2 2s\ ^2S$ |
| 108.0 | 0.5 | Li III $4p\ ^2P^\circ \rightarrow 1s\ ^2S$ (in second order) |
| 113.9 | 1 | Li III $3p\ ^2P^\circ \rightarrow 1s\ ^2S$ (in second order) |
| 242.9 | 1 | He II $4p\ ^2P^\circ \rightarrow 1s\ ^2S$ |

[a] Observed in absorption (Ref. 8).
[b] Observed in emission (Ref. 11).
[c] Observed in absorption (Ref. 6).
[d] Tentative assignment (Ref. 8).

the initial-state energy appears as kinetic energy of the ejected electron. The integrated intensity in the radiative autoionization tail is in good agreement with the 9% branching ratio calculated by Nicolaides and Beck.[5]

Additional features in the spectrum are given in Table II. These features include transitions in Li II and Li III as well as some radiative transitions from core excited odd-parity states which decay predominately by autoionization. The identification of the Lyman-$\alpha$ transitions in Li III and He II are supported by our observation of longer-wavelength series members (Li III $2p \rightarrow 1s$ at 135 Å and He II $3p \rightarrow 1s$ and $2p \rightarrow 1s$ at 256.3 and 303.8 Å, respectively) which are not shown in Fig. 2.

Only those features which are consistently reproduced are listed in Tables I and II. Although the numerical data delineate relative amplitudes somewhat better than does Fig. 2, the amplitudes of the smaller lines are somewhat uncertain.

The spectra obtained in emission are significantly less complex, and are often complementary to those obtained by absorption or ejected-electron spectroscopy. For example, although the strong 207.5-Å transition originates from the $1s2p^2\ ^2P$ level, this level is not observed in ejected-electron spectra.[9,10] However, the $1s2p^2\ ^2S$ and $1s2p^2\ ^2D$ levels, which have the same configuration and parity, are allowed to autoionize and so are seen in the ejected-electron spectra, and not observed here.

If we assume that the fine-structure components of the 207.5-Å transition lie beneath its Doppler linewidth (3.5 $cm^{-1}$), then based on its calculated oscillator strength[2,4,5] its cross section for stimulated emission is $3\times 10^{-14}$ $cm^2$, and about $10^{12}$ excited atoms per cubic centimeter are required for a gain of several percent per centimeter. This population must be attained in the 42 ps (calculated)[5] or 15 ps (measured)[3] lifetime. Two methods of pumping which allow much longer storage times are optical transfer from metastable quartet levels,[1] and two-photon optical pumping, where one of the photons is generated by laser-induced anti-Stokes emission near 199 Å in the $Li^+$ ion.[12,13] In any of these methods, an incident laser could be used to rapidly empty the terminal $(1s2p\ ^2P^\circ)$ laser level.

The authors acknowledge helpful discussions with T. Lucatorto, C. Bunge, R. Crossley, and A. Dalgarno, and the technical assistance of B. Yoshizumi. This work was supported by the U. S. Office of Naval Research.

[1] S. E. Harris, Opt. Lett. 5, 1 (1980).
[2] C. F. Bunge, Phys. Rev. A 19, 936 (1979).
[3] J. P. Buchet, M. C. Buchet-Poulizac, and H. G. Berry, Phys. Rev. A 7, 922 (1973).
[4] J. L. Fox and A. Dalgarno, Phys. Rev. A 16, 283 (1977).
[5] C. A. Nicolaides and D. R. Beck, Phys. Rev. A 17, 2116 (1978).
[6] D. L. Ederer, T. Lucatorto, and R. P. Madden, Phys. Rev. Lett. 25, 1537 (1970).
[7] T. J. McIlrath and T. B. Lucatorto, Phys. Rev. Lett. 38, 1390 (1977).

[8]A. M. Cantu, W. H. Parkinson, G. Tondello, and G. P. Tozzi, J. Opt. Soc. Am. 67, 1030 (1977).
[9]D. Rassi, V. Pejcev, and K. J. Ross, J. Phys. B 10, 3535 (1977).
[10]P. Ziem, R. Bruch, and N. Stolterfoht, J. Phys. B 8, L480 (1975).
[11]R. L. Kelly, U. S. Naval Research Laboratory Report No. 6648, 1968 (unpublished) (U. S. GPO, Washington, D. C.).
[12]S. E. Harris, Appl. Phys. Lett. 31, 498 (1977).
[13]L. J. Zych, J. Lukasik, J. F. Young, and S. E. Harris, Phys. Rev. Lett. 40, 1493 (1978).

# Electron Energy Transport into Layered Targets Irradiated by $CO_2$-Laser Light

J. C. Kieffer, H. Pépin, F. Martin, P. Church, and T. W. Johnston
*Institut National de la Recherche Scientifique–Energie, Université du Québec, Varennes, Québec J0L2P0, Canada*

and

R. Decoste
*Institut de Recherche d'Hydro-Québec, Varennes, Québec J0L2P0, Canada*
(Received 22 January 1980)

Inward energy transport ranges in layered targets have been measured as a function of the irradiance of short-pulse $CO_2$-laser light. As electromagnetic ponderomotive effects become important, the penetration of thermal electrons is sharply reduced and the penetration of suprathermal electrons increases much more slowly with irradiance. These results are discussed in the context of target implosions driven by suprathermal electrons.

PACS numbers: 52.50.Jm

Efficient energy transport from the absorption region to the core of the pellet shell target is needed in laser fusion to produce the inward shell acceleration and subsequent thermonuclear-burn conditions. Sufficient energy transport by thermal electrons has been demonstrated for 1.06-$\mu$m lasers at moderately low irradiance.[1] Longer-wavelength lasers, however, produce abundant suprathermal electrons leaving much less energy available for thermal electron transport. It has then been suggested that the hot-electron penetration into the target could become an alternate energy transport mechanism for 10.6-$\mu$m lasers at high target irradiance.[2] Lateral transport of hot electrons has been observed[3] with a 10.6-$\mu$m-wavelength laser at somewhat higher irradiances than ours, but we do not address that problem here. In this Letter, we report observations of the depth of heat transport by both thermal and suprathermal electrons for two different irradiance regimes. At the lower irradiances, both the thermal- and suprathermal-electron penetration are increasing with irradiance, as expected. However, at the higher irradiances, with the onset of electromagnetic ponderomotive force effects, the thermal-electron penetration decreases sharply while the suprathermal-electron penetration increases only weakly with irradiance. These results are encouraging for the fusion application mentioned above.

These experiments were carried out with a $CO_2$-laser beam (10.6 $\mu$m wavelength) incident on planar layered targets. The *S*-polarized laser pulse, 1.5 nsec in duration (full width at half maximum) with a prepulse-to-main-pulse contrast ratio $<10^{-6}$, was focused on target by an $f/1.5$ off-axis parabolic mirror. With an infrared film sensitizing technique,[4] the half-energy spot diameter was measured to be 130 $\mu$m, essentially independent of laser irradiance and without any hot spots.

To ascertain the importance of the electromagnetic ponderomotive force effects on the transport and interaction physics, we covered the range of target irradiance corresponding to a variation of the parameter $\gamma = v_0/v_t$ (electron oscillatory to cold thermal velocity) from 0.2 to 1.5. This range covers the transition from a regime of "weak" ($\gamma < 1$) to "moderate" ($\gamma > 1$) plasma-density profile modification.[5] This transition is clearly illustrated in Fig. 1 by typical interferograms obtained with a 35-psec ruby-laser pulse synchronized and time delayed with respect to the $CO_2$ laser. At lower irradiances ($\gamma < 1$), Abel inversion of the well-separated fringes yields an on-axis density-gradient scale length of about 35 $\mu$m. At higher irradiances ($\gamma > 1$), the density scale length is reduced to less